computation

MDPI

Article

Density Functional Theory Study of Metal and Metal-Oxide Nucleation and Growth on the Anatase TiO_2(101) Surface

Leila Kalantari *, Fabien Tran and Peter Blaha

Institute of Materials Chemistry, Vienna University of Technology, Getreidemarkt 9/165-TC, A-1060 Vienna, Austria; tran@theochem.tuwien.ac.at (F.T.); pblaha@theochem.tuwien.ac.at (P.B.)
* Correspondence: leila.kalantari@tuwien.ac.at

Abstract: Experimental studies have shown the possible production of hydrogen through photocatalytic water splitting using metal oxide (MO_y) nanoparticles attached to an anatase TiO_2 surface. In this work, we performed density functional theory (DFT) calculations to provide a detailed description of the stability and geometry of M_xO_y clusters M = Cu, Ni, Co, Fe and Mn, x = 1–5, and y = 0–5 on the anatase TiO_2(101) surface. It is found that unsaturated 2-fold-coordinated O-sites may serve as nucleation centers for the growth of metal clusters. The formation energy of Ni-containing clusters on the anatase surface is larger than for other M clusters. In addition, the Ni_n adsorption energy increases with cluster size n, which makes the formation of bigger Ni clusters plausible as confirmed by transition electron microscopy images. Another particularity for Ni-containing clusters is that the adsorption energy per atom gets larger when the O-content is reduced, while for other M atoms it remains almost constant or, as for Mn, even decreases. This trend is in line with experimental results. Also provided is a discussion of the oxidation states of M_5O_y clusters based on their magnetic moments and Bader charges and their possible reduction with oxygen depletion.

Keywords: DFT; anatase TiO_2(101) surface; adsorption energy; Bader charge

check for updates

Citation: Kalantari, L.; Tran, F.; Blaha, P. Density Functional Theory Study of Metal and Metal-Oxide Nucleation and Growth on the Anatase TiO_2(101) Surface. *Computation* **2021**, *9*, 125. https://doi.org/10.3390/computation9110125

Academic Editor: Henry Chermette

Received: 12 October 2021
Accepted: 5 November 2021
Published: 19 November 2021

Publisher's Note: MDPI stays neutral with regard to jurisdictional claims in published maps and institutional affiliations.

Copyright: © 2021 by the authors. Licensee MDPI, Basel, Switzerland. This article is an open access article distributed under the terms and conditions of the Creative Commons Attribution (CC BY) license (https://creativecommons.org/licenses/by/4.0/).

1. Introduction

The over-exploitation of the fossil energies leads to a significant increase of CO_2 in the atmosphere, resulting in severe climate problems. It is therefore absolutely necessary to replace them by alternative energy sources. When using sun light as energy source, however, materials with specialized properties are necessary, and TiO_2 is such a versatile material that has numerous applications in catalysis, photocatalysis, and solar energy [1]. TiO_2 crystallizes in three major different structures: rutile (tetragonal), anatase (tetragonal) and brookite (rhombohedral). Other structures exist as well, as for example cotunnite, that has been synthesized at high pressures and is one of the hardest polycrystalline materials known. However, only rutile and anatase play an important role in the applications of TiO_2. A well-suited model compound for photocatalytic water splitting is anatase. It has a slightly larger band gap than rutile (∼3.0 eV for rutile and ∼3.2 eV for anatase) [2–6] and shows better performance [7], since it also has a longer electron-hole pair life time, which makes anatase more suitable for photocatalytic applications [8]. To improve the water splitting photocatalyst activity, the use of co-catalysts is necessary and the most widely used are Pt and Pd for photocatalytic reduction, and IrO_2 and RuO_2 for the oxidation of water. However, these are expensive materials based on rare noble metals. To achieve large-scale industrial applications of photocatalytic water splitting, the development of new co-catalysts based on cheap and widely available elements remains an important issue. With regard to novel abundant co-catalysts for photocatalytic water splitting, research efforts focus on 3*d* transition metals (M) oxides, which are known for their excellent catalytic properties and applications in industry, research and nature.

Recently, small clusters of M oxides were produced by deposition of M-acetylacetonate precursors on TiO_2 and subsequent calcination in air. In particular, the Ni (and Cu) nanoparticles showed pronounced activities for water splitting, but little is known about the atomic structure of these nanoparticles [9]. This inspired the present work, where we used density functional theory (DFT) [10,11] to study possible adsorption sites of a 3*d* transition metal atom (Cu, Ni, Co, Fe, and Mn), which can be the nucleation sites for bigger M clusters (2 to 5 atoms) or M oxides clusters on TiO_2(101) anatase, the lowest-energy surface of anatase [12]. There are a couple of previous theoretical works on the M adsorption on anatase, studying single M atom adsorption and diffusion [13], or the adsorption of small Ni [14] or Cu and Cu-oxide [15,16] clusters. A nice review related to this topic is given by Zhou and Dong [17]. However, note that most of these calculations used a generalized gradient approximation (GGA) in DFT for the correlated 3*d* electrons, which may not be accurate enough.

2. Methods

Spin-polarized DFT calculations of the adsorption of M_xO_y clusters (M = Cu, Ni, Co, Fe or Mn, $x = 1, 2, 3, 5$, and $y = 0, 1, 2, 3, 4, 5$) on the TiO_2(101) surface were performed using the full-potential augmented plane wave plus local orbitals method [18,19] as implemented in the WIEN2k code [20,21]. We employed the PBEsol exchange-correlation functional [22], which is a GGA and yields lattice parameters of bulk anatase TiO_2, $a = b = 3.77$ Å and $c = 9.54$ Å that are in good agreement with experimental data [23]. In order to treat the correlated 3*d* electrons of the M atoms a Hubbard U correction was used [24]. We used $U_{\text{eff}} = U - J$ of 5 eV for Cu, Ni, and Co and 4 eV for Mn and Fe. These values are deliberately chosen smaller than what is typically used in strongly correlated oxides, since in our case also less ionic (metallic) clusters were investigated and the correlation may not be always so strong. We note that small changes of U_{eff} would not affect our basic results and conclusions.

The (101) surface was modeled by a symmetric slab with a thickness of three layers of TiO_2 (see Figure 1, where only one layer is shown for better visibility) and a vacuum region of 16 Å between the slabs. In order to reduce the interactions between the adsorbed clusters in neighboring cells a 3×1 supercell was used for all surfaces with adsorbed M atoms. Moreover, such a supercell is also helpful to release the interfacial strain energy and find more stable configurations. A $2 \times 2 \times 1$ Γ-centered mesh of **k**-points is used during relaxation (a $5 \times 4 \times 1$ mesh for the final results) and a basis-set size corresponding to $R_{\text{MT}}^{\text{min}} K_{\text{max}} = 7$, where $R_{\text{MT}}^{\text{min}}$ is the smallest atomic sphere radius and K_{max} the largest reciprocal lattice vector, was used. All surface models were relaxed until all residual forces were below 1 mRy/bohr.

Consistent R_{MT} and $R_{\text{MT}}^{\text{min}} K_{\text{max}}$ values have been used for calculating the adsorption energy E_{ads} of clusters on anatase surface, which is defined as

$$\begin{aligned} E_{\text{ads}} &= \frac{1}{x+y}[E(\text{TiO}_2(101)) + xE(\text{M}) + y\frac{1}{2}E(\text{O}_2) \\ &\quad -E(\text{M}_x\text{O}_y/\text{TiO}_2(101))], \end{aligned} \tag{1}$$

where $E(\text{M})$ and $E(\text{O}_2)$ are the total energies of the free M atom and an O_2 molecule, and $E(\text{TiO}_2(101))$ is for the bare TiO_2(101) surface. Bader's quantum theory of atoms in molecules [25] was used to calculate the atomic magnetic moments and charges.

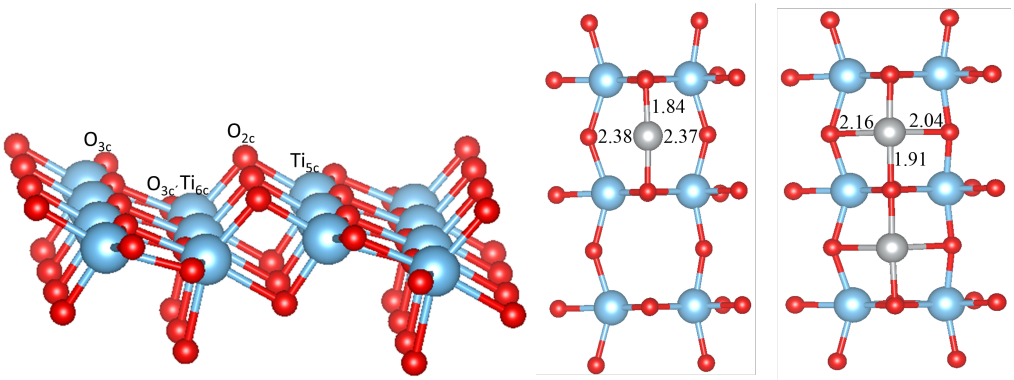

Figure 1. Side and top views of the top-most layer of the TiO_2(101) surface (in the 3×1 supercell) with a single adsorbed Ni atom (middle) and two Ni atoms (right structure). Red, blue and gray spheres correspond to O, Ti and Ni atoms, respectively. Selected Ni-O bond distances (in Å) are also given. O_{3c} and $O_{3c'}$ are threefold coordinated oxygen with two Ti_{6c} and one Ti_{5c}, and two Ti_{5c} and one Ti_{6c} nearest neighbors, respectively.

3. Results and Discussion

3.1. Perfect Anatase TiO_2(101) Surface

As shown in Figure 1, the anatase TiO_2(101) surface has a stepped structure. Threefold coordinated O atoms (O_{3c} and $O_{3c'}$) and sixfold coordinated Ti atoms (Ti_{6c}) are fully saturated and have bulk-like coordination, whereas the twofold O_{2c} and fivefold Ti_{5c} atoms are under-coordinated. The O_{2c} atoms are located at the ridges of the saw-tooth-like structure, and after optimization they relax inwards by ∼0.16 Å with respect to bulk TiO_2. The three-fold coordinated O_{3c} and $O_{3c'}$ atoms relax outwards by ∼0.07 Å, while the Ti_{5c} and Ti_{6c} atoms relax inwards by ∼0.15 Å and ∼0.16 Å respectively, so that the surface exhibits a slightly buckled structure.

3.2. Pure Metal Clusters on the Anatase TiO_2(101) Surface

Upon calcination of the M-acetylacetonate precursors, single M atoms may adsorb, diffuse and form larger clusters and finally oxidize on the surface. It is thus natural to study as a first step the possible adsorption sites of a single M atom or a small cluster. We have considered several possible initial configurations of the adsorbed metal atoms and clusters M_x with $x = 1, 2, 3$, and 5. The most stable structures, which are the same for all M (Cu, Ni, Co, Fe or Mn), are presented in Figures 1–3 in the case of Ni clusters with $x = 1, 2$ and 5. The nearest-neighbor distances are shown in Table 1, while the adsorption energy E_{ads} and magnetic moment are available in Table 2.

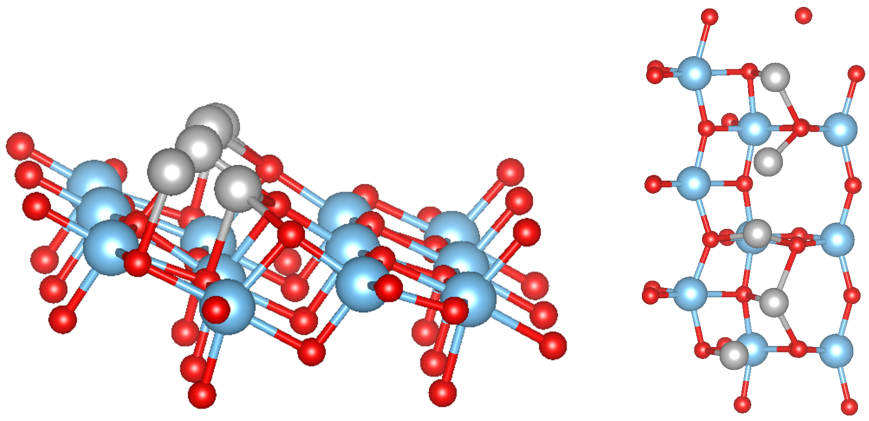

Figure 2. Side and top views of the top-most layer of the TiO_2(101) surface with an adsorbed Ni_5 cluster in a chain-like structure. The color coding is as in Figure 1.

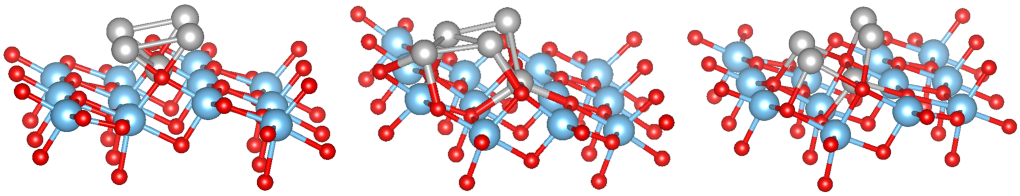

Figure 3. Side view of the starting (**left**) and relaxed structures of Ni_5 (**middle**) and Fe_5 clusters (**right**) adsorbed on the TiO_2(101) surface in a crystalline structure. The color coding is as in Figure 1.

Table 1. Shortest M-O bonds (in Å) between a M atom (of the pure metal clusters adsorbed on the TiO_2(101) surface) and O atoms (O_{2c} and O_{3c}) of TiO_2. M_5(1) and M_5(2) refer to chain-like and crystalline structures, respectively, and Mn_5(2a) corresponds to a bcc like structure with antiferromagnetic configuration. The results for different M atoms are separated by semi-colons. "(2)" means two bonds of same length.

	MO Bulk	**MO_{2c} at the Surface**	**M-O_{3c} at the Surface**
TiO_2-Cu	(CuO)1.97/(Cu_2O)1.86	1.87(2)	2.33, 2.47
TiO_2-Cu_2		(1.88, 1.89); (1.88, 1.89)	(2.34, 2.52); (2.34, 2.52)
TiO_2-Cu_3		1.90(2); 1.90(2); 1.90(2)	(2.28, 2.46); (2.28, 2.46); (2.29, 2.46)
TiO_2-Cu_5(1)		1.97; 2.11; (2.09, 2.10); (2.04, 2.15); 2.83	(2.81, 2.71); (2.31, 2.90); 2.30; 2.42; -
TiO_2-Cu_5(2)		1.86; -; -; 2.94; 1.86	-; -; -; 2.00; 2.75
TiO_2-Ni	2.08	1.84(2)	2.37, 2.38
TiO_2-Ni_2		(1.91, 1.92); (1.91, 1.92)	(2.04, 2.16); (2.04, 2.16)
TiO_2-Ni_3		1.89(2); 1.89(2); 1.89(2)	(2.02, 2.31); (2.02, 2.31); (2.02, 2.31)
TiO_2-Ni_5(1)		2.02; 1.99; (2.04, 2.22); (2.13, 2.46); 2.86	2.04; 2.75; 2.10; 2.04; 2.05
TiO_2-Ni_5(2)		(1.96, 1.94); 2.13; 1.98; -; 2.07	(2.04, 2.16); -; -; 2.01; 2.07
TiO_2-Co	2.13	1.89(2)	2.03, 2.71
TiO_2-Co_2		1.97(2); (1.88, 1.89)	(2.03, 2.04); (2.03, 2.76)
TiO_2-Co_3		(1.99, 2.00); (2.03, 1.91); (1.90, 2.02)	(2.05, 2.09); (2.04, 2.12); (2.04, 2.29)
TiO_2-Co_5(1)		2.08; 2.30; (2.06, 2.09); (2.03, 2.06); 2.06	(2.15, 2.30); 2.04; 2.13; 2.15; 2.86
TiO_2-Co_5(2)		2.02; -; 1.91; 2.90; 2.07	2.09; -; -; 1.96; 2.19
TiO_2-Fe	2.16	1.89(2)	2.08, 2.23
TiO_2-Fe_2		(1.88, 1.91); (1.88, 1.91)	(2.10, 2.11); (2.10, 2.11)
TiO_2-Fe_3		1.88(2); 1.88(2); 1.88(2)	(2.11, 2.14); (2.11, 2.14); (2.11, 2.14)
TiO_2-Fe_5(1)		2.03; 2.09; (2.00, 2.09); (2.05, 2.15); 2.98	(2.21, 2.25); 2.09; 2.14; 2.06; 2.02
TiO_2-Fe_5(2)		(2.06, 2.05); 2.04; 2.04; 2.22; 2.25	(2.14, 2.04); -; -; 2.11; 2.08
TiO_2-Mn	2.22	1.93(2)	2.14, 2.30
TiO_2-Mn_2		1.94(2); 1.94(2)	(2.11, 2.28); (2.11, 2.28)
TiO_2-Mn_3		(1.91, 1.92); (1.92, 1.93); (1.92, 1.93)	(2.16, 2.30); (2.16, 2.27); (2.16, 2.27)
TiO_2-Mn_5(1)		2.17; 2.19; (2.03, 2.08); (2.10, 2.03); 3.27	2.12; 2.13; 2.16; 2.16; 2.07
TiO_2-Mn_5(2)		(2.02, 2.02); 2.08; 2.08; 2.17; 2.18	(2.03, 2.04); -; -; 2.09
TiO_2-Mn_5(2a)		(2.14, 2.15); 2.09; 2.09; 2.07; 2.07	2.15; -; -; 2.15; 2.16

A single adsorbed M atom prefers to adsorb at the bridge site between two unsaturated oxygens (O_{2c}) atoms, similar as found in previous studies [13,14]. The corresponding M-O bond length (it is the shortest for Ni, 1.84 Å) follows in general the trend found in the bulk M oxides (except for the Cu-O and Ni-O distances, which are interchanged), but in all cases is much shorter (and therefore indicates a stronger bonding) than in the bulk MO (e.g., 2.08 Å in NiO). The particular short bond distance for Ni goes hand in hand with the O_{2c}-Ni-O_{2c} bond angle, which reaches 177° and forms a nearly linear bond, while for the other metals this varies from 167° (Fe) to 150° (Co). On the other hand the two larger M-O_{3c} bond distances are also almost equal (but very large) for Ni, but for all other M form a short and long bond in an asymmetric position (see Table 1). All M atoms except Cu possess a magnetic moment (see Table 2), where as expected Mn has the largest moment, while it is the smallest for Ni. It should be noted that PBEsol without *U* would lead to a

non-magnetic Ni atom and the moments for the other M would be smaller but still sizeable. The adsorption energy on the TiO_2(101) surface (Table 2) is the largest for Ni (3.46 eV) and the smallest for Cu (2.24 eV). Comparing our results with literature the adsorption energy of Ni is 0.4 eV larger than in references [13,14] and the Ni position is symmetric with respect to the O_{3c} atoms. On the other hand, our calculated adsorption energy for Fe is 0.7 eV smaller than that in reference [13], while it agrees well for Cu and Co. These differences could arise due to the neglect in references [13,14] of a Hubbard U correction for the M atom or the use of pseudopotentials.

Table 2. Adsorption energy (in eV/atom) and atomic magnetic moment (in μ_B) for pure metal clusters adsorbed on the TiO_2(101) surface. $M_5(1)$ and $M_5(2)$ refer to the chain-like and crystalline structures, respectively, and Mn_5(2a) corresponds to the bcc structure with antiferromagnetic configuration. The cohesive energies for bulk MO are 2.75, 4.20, 3.72, 3.41, and 3.34 eV for Cu, Ni, Co, Fe, and Mn, respectively.

Solid	E_{ads}	Magnetic Moment
TiO_2-Cu	2.24	0
TiO_2-Cu_2	2.08	0
TiO_2-Cu_3	1.99	0
TiO_2-$Cu_5(1)$	1.90	0
TiO_2-$Cu_5(2)$	2.26	0
TiO_2-Ni	3.46	0.25
TiO_2-Ni_2	4.11	0.97(2)
TiO_2-Ni_3	3.94	0.98(3)
TiO_2-$Ni_5(1)$	3.68	1.66; 1.08; 1.31; 1.11; 1.35
TiO_2-$Ni_5(2)$	4.49	−0.97; 1.22; 0.74; −1.10; 0.87
TiO_2-Co	3.19	2.12
TiO_2-Co_2	3.04	2.12; 2.11
TiO_2-Co_3	3.00	2.15; 2.28; 2.28
TiO_2-$Co_5(1)$	2.73	2.03; 2.53; 2.52; 2.18; 2.44
TiO_2-$Co_5(2)$	2.87	2.34; 2.00; 2.66; 1.96; 2.04
TiO_2-Fe	2.71	3.61
TiO_2-Fe_2	2.57	3.51; 3.50
TiO_2-Fe_3	2.48	3.52(3)
TiO_2-$Fe_5(1)$	2.18	3.62; 3.79; 3.64; 3.48; 3.71
TiO_2-$Fe_5(2)$	2.03	3.00; 3.75; 3.72; 3.58; 3.57
TiO_2-Mn	2.40	4.66
TiO_2-Mn_2	2.19	4.66(2)
TiO_2-Mn_3	2.08	4.61; 4.61; 4.63
TiO_2-$Mn_5(1)$	1.78	4.90; 4.94; 4.66; 4.66; 4.83
TiO_2-$Mn_5(2)$	1.10	0.45; 5.00; 4.99; 4.57; 4.57
TiO_2-Mn_5(2a)	1.44	4.90; −5.04; 5.03; −4.73; −4.73

If 2 or 3 M atoms are adsorbed on the surface, the most stable structures are still obtained when the M atoms sit at the O_{2c} bridge sites (the structure on the right side in Figure 1 shows 2 M atoms adsorbed on the surface), very similar to a single atom adsorption. Interestingly, for all M atoms except Ni the adsorption energy per M atom decreases slightly (Figure 4 and Table 2). For Ni it increases by 0.65 eV. The reason seems to be that the Ni atom is smaller than the others and an almost linear chain fits perfectly for Ni but not in the other cases, where this additional strain reduces E_{ads} slightly. Most magnetic moments remain unchanged, except for Ni, where it increases to 0.97/0.98 μ_B. In our 3 × 1 supercell, 3 M atoms form an infinite linear chain of M-O_{2c} pairs.

For 5 adsorbed M atoms, we tried several different starting structures in the 3 × 1 supercell. The most promising structures are based on the chain-like structure with 2 additional atoms (labelled $M_5(1)$, see Figure 2) or a structure with a more "crystalline type" nucleated on a single M bridge atom (labelled $M_5(2)$, see Figure 3). The additional 2 atoms

"destroy" the symmetric chain-like 3-atom structure above the O_{2c} atoms forming a quite irregular array of M atoms with bonds to O_{2c}, O_{3c} and $O_{3c'}$ atoms. Still this structure seems to be the most stable for Fe and Mn although E_{ads} is smaller than for less M atoms. The crystalline $M_5(2)$ structures behave very differently for the bcc metals Mn and Fe and the fcc metals Co, Ni and Cu. While for the former the cluster structure stays basically close to the starting one and form a "bcc" like cluster (Figure 3), for the latter the cluster rearranges and can be considered as a nucleus for an fcc like cluster. In fact, their E_{ads} is larger than for the corresponding chain-like $M_5(1)$ structures and for Ni and Cu even the highest within the series.

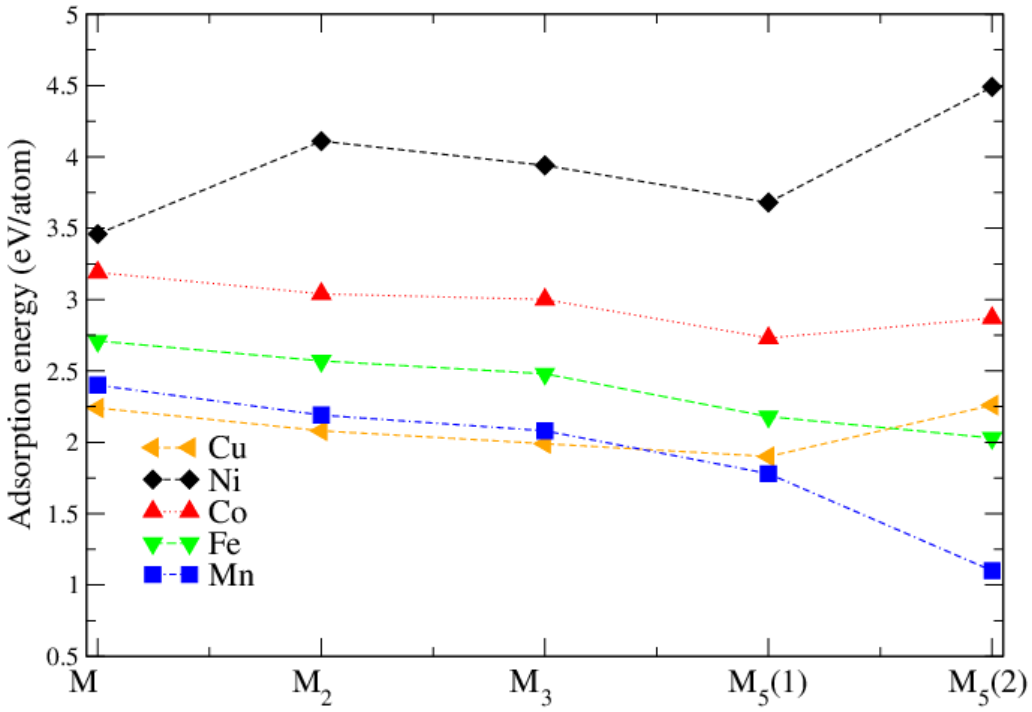

Figure 4. Adsorption energy (in eV/atom) for different metal clusters M_x. $M_5(1)$ and $M_5(2)$ correspond to chain-like and crystalline structures, respectively.

For Mn_5 in a crystalline bcc structure, we also started from different antiferromagnetic configurations (labelled Mn_5(2a)), but the adsorption energies were not much larger than in the ferromagnetic case.

The partial density of states (PDOS) for the TiO_2(101) surface and for the energetically most favorable configuration of one metal atom on the surface are shown in Figure 5. For the TiO_2(101) surface, both the valance band maximum (VBM) and the conduction band minimum (CBM) are composed of a mixture of O-2*p* and Ti-3*d* states, with the CBM having mostly 3*d* character while the VBM has more O-2*p* character, which indicates a mixed ionic and covalent bonding. After adsorption of a M atom on the anatase TiO_2(101) surface, the Fermi level moves to the conduction band and the system becomes formally metallic. In the case of adsorbed Cu and Ni atoms, almost all the *d* states of Cu/Ni are concentrated in the band gap below the Fermi energy, and they slightly hybridize with the O-*p* and Ti-*d* states of the Ti and O atoms which are the closest to the Cu/Ni atom. With an adsorbed Co, Fe, or Mn atom the *d* states are not only in the band gap but also show a peak at the VBM for spin-up and inside the conduction band for spin-down states.

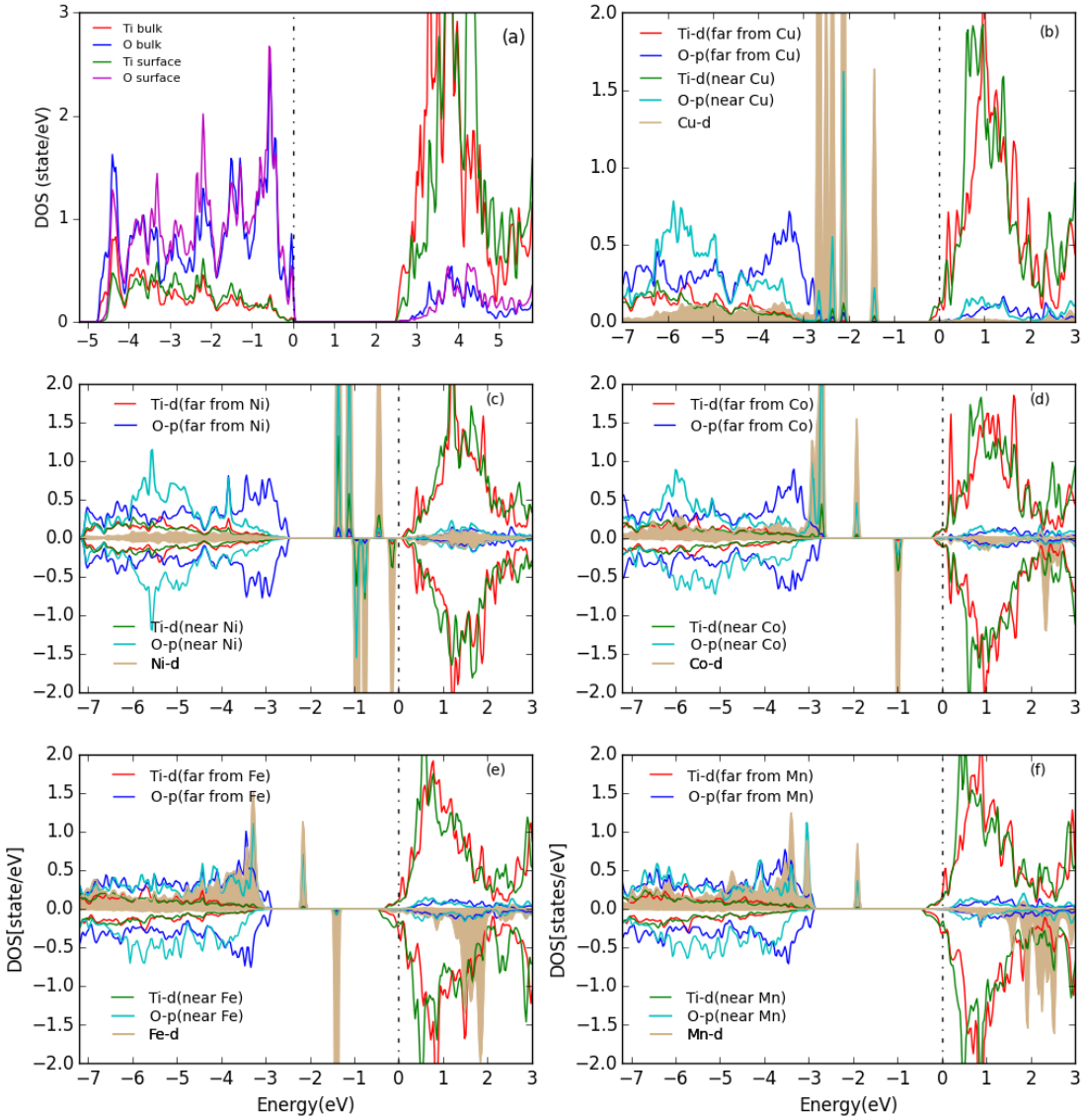

Figure 5. PDOS for (**a**) the bare TiO_2(101) surface and (**b**–**f**) for one metal atom adsorbed on the TiO_2(101) surface. The Fermi level is indicated by a vertical dashed line. All Ti and O PDOS are from surface atoms. The *d* partial DOS of the metals are scaled down by a factor of 3. The plots are aligned at the TiO_2 CBM and the Fermi energy is set at 0 eV.

3.3. M_xO_y on the Anatase TiO_2(101) Surface

Turning now to the adsorption of metal-oxides clusters M_xO_y on the anatase TiO_2(101) surface, several 2D and 3D (starting) configurations among the numerous possible ones were considered. Some of the most stable structures are shown in Figures 6 and 7, and the adsorption energies are shown in Table 3 for the Ni_xO_y clusters. It can be seen that E_{ads} is almost constant with the increase of cluster size indicating that bigger Ni clusters can easily be formed on the anatase TiO_2(101) surface, which is in agreement with the experimental result [9]. The most favorable structure is $Ni_{10}O_9$ with a NaCl like structure (shown in Figure 7).

It was found experimentally [9] that the oxidation state of the M atoms changed after a hydrogen evolution reaction (HER) experiment. In order to study the M oxidation state theoretically, we started from the chain-like M_5 clusters (Figure 6) and added oxygen atoms systematically until a fully oxidized M cluster has been obtained. Figure 8 compares the adsorption energy of different M_5O_y M oxide clusters on the surface and also includes for comparison the cohesive energy of the bulk pure metals and bulk metal monoxides. It can

be seen that, among all metal-oxide clusters, Ni_xO_y have the highest adsorption energy. All adsorption energies are lower than the cohesive energies of the corresponding bulk monoxide and the pure bulk metal. Thus they form non-crystalline clusters on the surface. It can be seen that Ni clusters are a bit more stable with less oxygen, while for the other metals the adsorption energy remains almost constant, or, in particular for Mn, is reduced with less oxygen. This is in agreement with experimental transition electron microscopy (TEM) results [9], where cluster formation was seen in particular for Ni. In addition, XPS on calcinated NiO_x-TiO_2 samples shows mainly Ni^{2+}, but after HER experiments a substantial increase of Ni^0 compared to Ni^{2+} appears. On the other hand, XPS on MnO_x-TiO_2 samples shows only Mn^{2+}, even after the HER experiments.

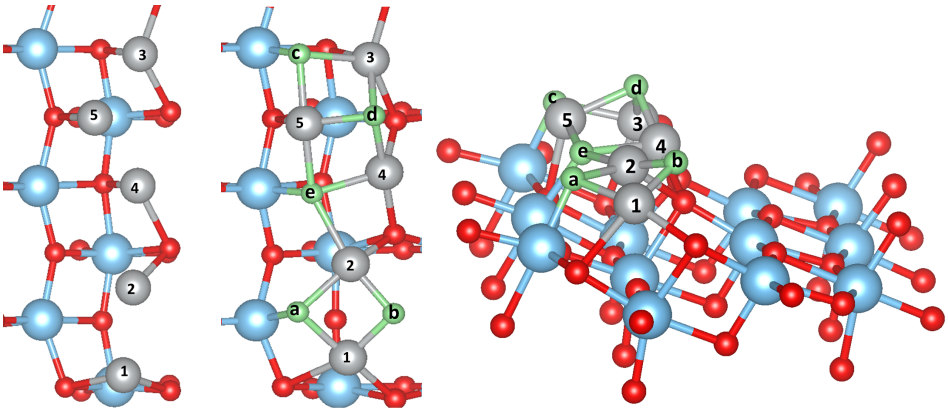

Figure 6. Top view of the Ni_5 cluster (**left**) and, top and side view of Ni_5O_5 cluster (**middle** and **right**) adsorbed on TiO_2(101) surface in chain-like structure. Red, blue, gray and green spheres correspond to O, Ti, Ni and added O, respectively. From Ni_5 to Ni_5O_5, the O atoms are added in the order O_a, O_b, O_c, O_d and O_e.

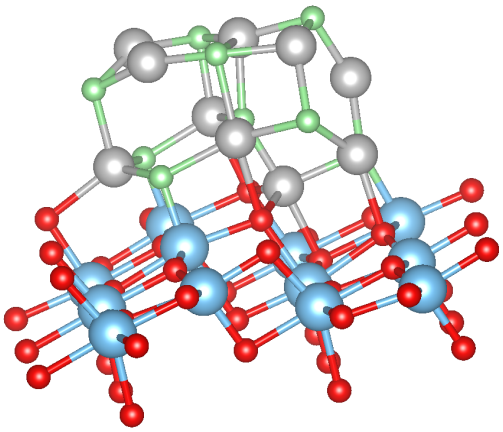

Figure 7. $Ni_{10}O_9$ cluster with a NaCl-like structure adsorbed on the TiO_2(101) surface. The color coding is as in Figure 6.

Theoretically, the oxidation state is more difficult to estimate. One can use for instance Bader's method [26], which uses the electron density to calculate the gradient vector field and searches for surfaces of zero flux. The charge enclosed within this zero flux surface (basin) can be used to define the total electronic charge of an atom. It must be mentioned that one never gets the full nominal charges, but these Bader charges are always smaller than anticipated. In addition, in particular for open structures like surfaces, these charges may sometimes correlate more with the specific geometry and the distances and number of other atoms around the M atom. For transition-metal atoms, the magnetic moment can also be a good indication of the charge state in some cases. For instance, only Cu^{2+} ions possess a magnetic moment, while both Cu^+ and neutral Cu are non-magnetic. Similarly, one

can quite well distinguish, e.g., Fe^{2+} and Fe^{3+} based on their smaller or larger magnetic moments (provided they remain in high-spin states). The magnetic moments and the Bader charges of each atom in M_5O_yclusters are shown in bar charts in Figures 9 and 10. The largest magnetic moments for each M atom increase as expected from 0.6 μ_B for Cu^{2+} to 1.6, 2.6, 3.7 and 4.9 μ_B in the series Ni, Co, Fe and Mn. This is due to the number of spin-down 3*d* electrons that gets reduced when dealing with high-spin states and fully occupied spin-up states.

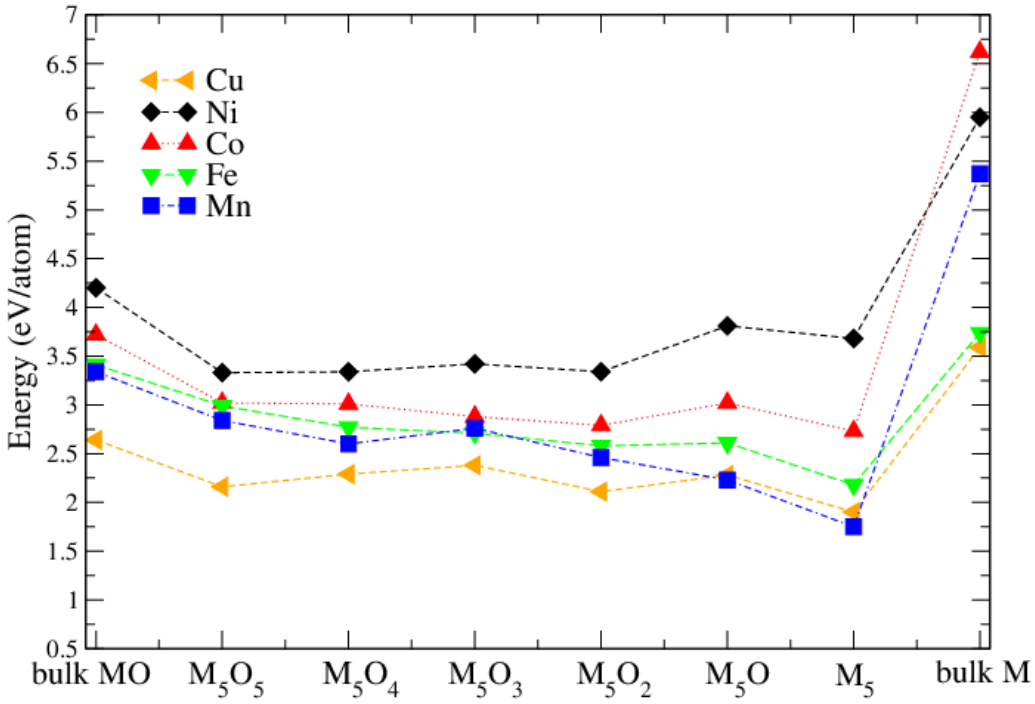

Figure 8. Adsorption energy (in eV/atom) of M_xO_y clusters on the TiO_2(101) surface. Also shown is the cohesive energy of bulk MO (left-most data) and bulk M (right-most data).

Table 3. Adsorption energy (in eV/atom) of Ni_xO_y clusters on TiO_2(101) surface. The largest values are in bold.

Cluster	E_{ads}
NiO(1)	**3.55**
NiO(2)	3.14
NiO(3)	3.19
NiO(4)	3.14
Ni_2O_2(1)	3.07
Ni_2O_2(2)	2.59
Ni_2O_2(3)	**3.58**
Ni_3O_3(1)	3.32
Ni_3O_3(2)	3.17
Ni_3O_3(3)	2.75
Ni_3O_3(4)	**3.51**
Ni_4O_4(1)	**3.42**
Ni_4O_4(2)	2.87
Ni_5O_5	**3.35**
$Ni_{10}O_9$	**3.63**

For the charge state of Cu clusters, both methods mentioned above give quite reliable results. Bader charges of about one and magnetic moments of 0.6 μ_B indicate Cu^{2+}, while Bader charges of 0.6 indicate Cu^{+} and even smaller Bader charges neutral Cu, both with vanishing magnetic moments. Apparently, in the fully oxidized cluster all Cu are in the 2+ charge state, while removal of an O_e atom (see Figure 6) leads to a drastic reduction of the charge state of the neighboring Cu_4 and Cu_5 atoms.

For Ni, however, the situation is more complicated. Even in the fully oxidized cluster some Ni moments are completely quenched because the Ni-O bond length (1.77 Å) is for these Ni atoms much smaller than for the magnetic ions (1.97 Å) and it is difficult to estimate the charge states based on the magnetic moment. On the other hand the Bader charges show a very systematic decrease with oxygen removal, and the experimentally observed increase of neutral Ni correlates reasonably with these Bader charges. Going to the extreme case of Mn, the magnetic moments stay almost constant around 5 μ_B indicative of Mn^{2+} in a high-spin state in agreement with experiment. The Bader charges are less convincing, but nevertheless they never indicate a neutral charge state of a Mn atom.

In order to get more information about the electronic structure, the PDOS of various Ni-O clusters is shown in Figure 11. For a Ni_5 cluster (Figure 11b) we see a wide range of Ni-*d* states within the gap of TiO_2, but also some spin-up states mixed into the O-2*p* valence band and some spin-down states in the empty conduction band, indicating the different bonding situation of the different Ni atoms. Upon oxidation a more pronounced formation of upper and lower Hubbard bands can be seen and the remaining Ni-*d* states in the gap sharpen until for the $Ni_{10}O_9$ cluster (Figure 11f) quite sharp Ni-*d* states of (distorted) e_g and t_{2g} character appear similar as in bulk NiO.

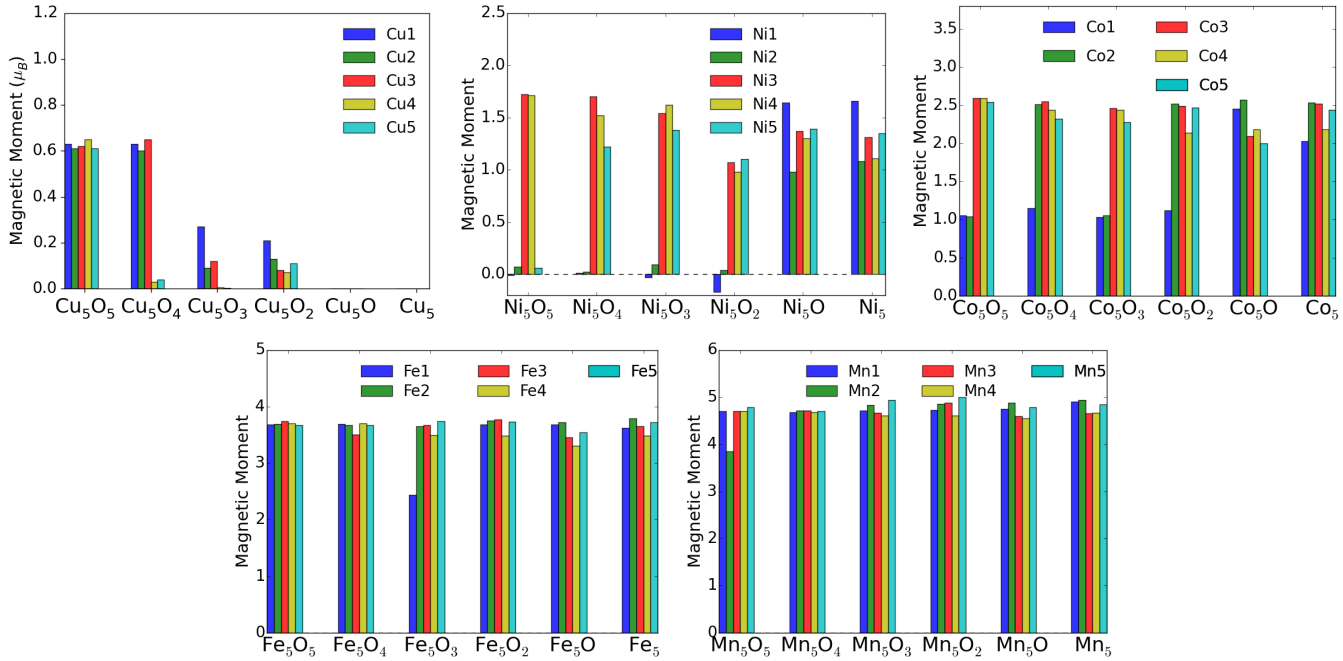

Figure 9. Atomic magnetic moments (in μ_B) of M atoms in M_xO_y clusters adsorbed on TiO_2(101) surface.

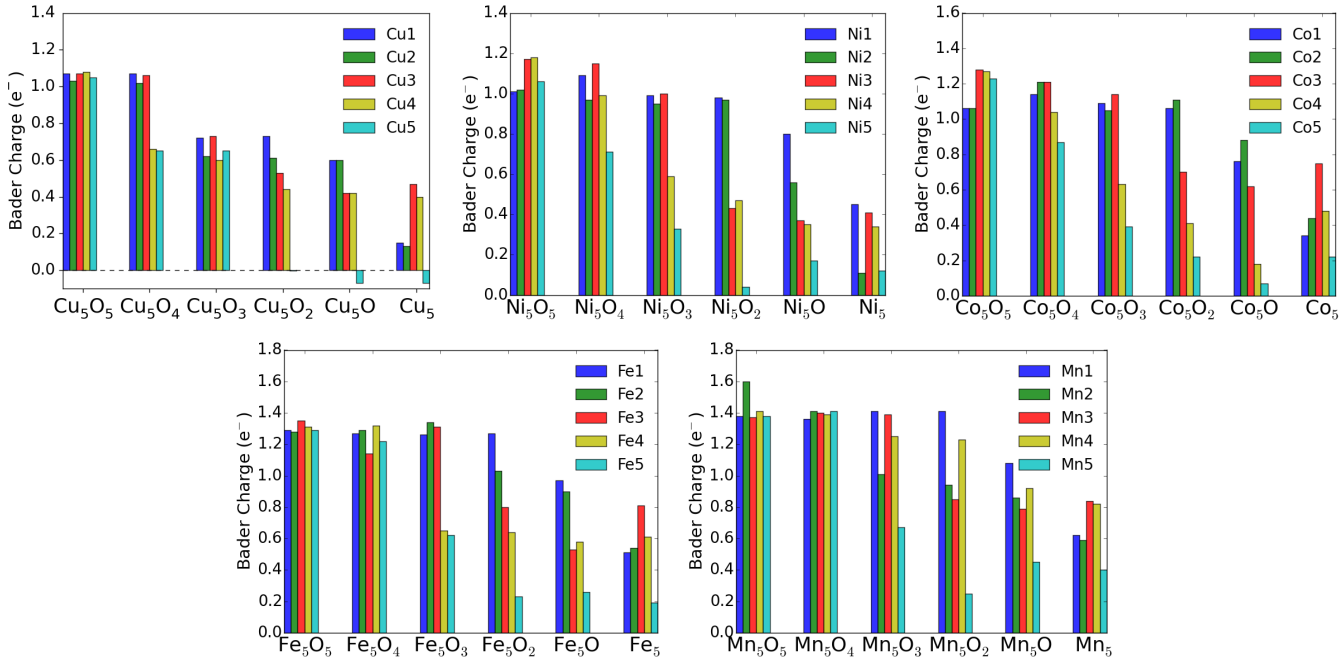

Figure 10. Bader charges of M atoms in M_xO_y clusters adsorbed on TiO_2(101) surface.

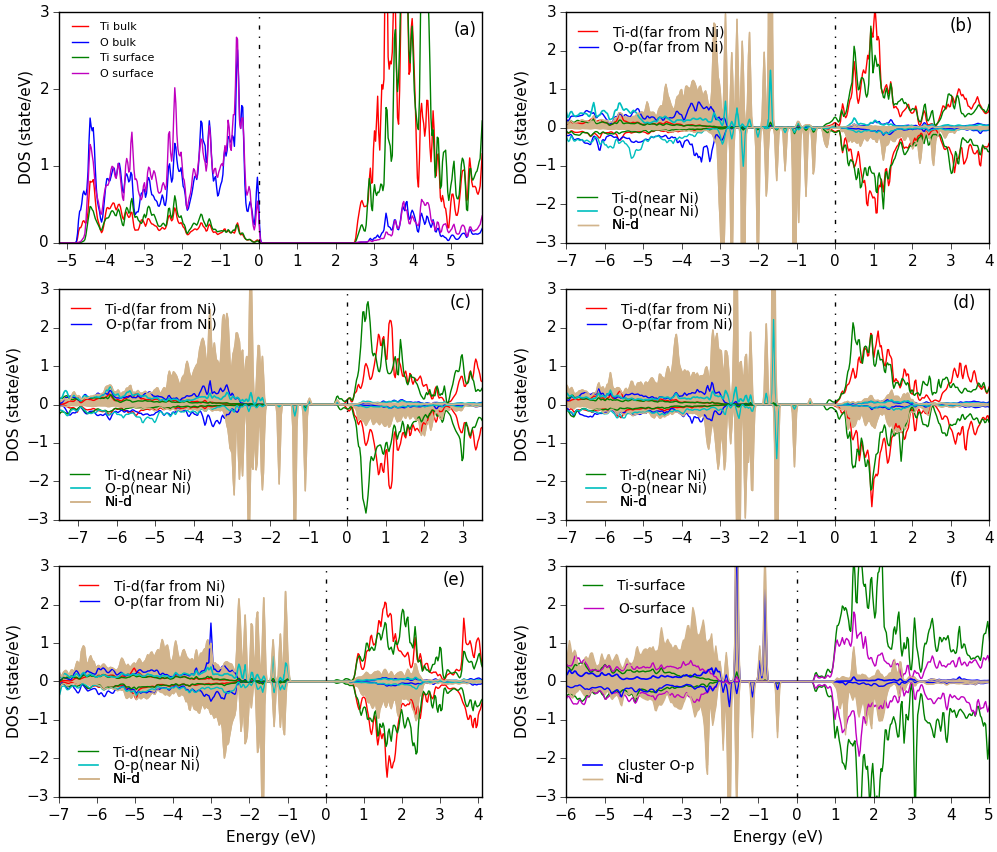

Figure 11. PDOS for (**a**) the bare anatase TiO_2(101) surface, showing the surface atoms and the bulk-layer states, (**b**) Ni_5, (**c**) Ni_5O, (**d**) Ni_5O_3, (**e**) Ni_5O_5 clusters in chain-like structures and (**f**) a $Ni_{10}O_9$ cluster with NaCl-like structure adsorbed on the surface. All Ti and O PDOS are from surface atoms only. The Ni PDOS is shaded. The plots are aligned at the TiO_2 CBM and the Fermi energy is set at 0 eV.

4. Summary and Conclusions

Spin-polarized DFT calculations were carried out to investigate possible stable structures of five different transition metal clusters, namely Cu, Ni, Co, Fe and Mn adsorbed on the anatase TiO_2(101) surface. The adsorption site for single atoms is in all cases the bridge site between two unsaturated oxygen (O_{2c}) atoms. We found that among all tested metals Ni has the largest adsorption energy, and for all metals except Ni the adsorption energies decrease with increased number of adsorbed atoms, so that probably only Ni prefers to form bigger clusters on the TiO_2 surface in agreement with experimental TEM results [9]. Clusters with five M atoms can form either a fcc-like structure (Cu, Ni, Co) or still remain in a chain-like structure (Fe, Mn) as is common for smaller clusters.

We also studied several oxidized metals clusters M_xO_y, and in order to get more information on the charge state of the M atom a systematic study of M_5O_y (y = 0–5) clusters on the TiO_2(101) surface was made. We found that Ni forms more stable structures with reduced oxidation, while for the other metals the adsorption energy is almost constant or is reduced. An analysis of the Bader charges and magnetic moments allows to reveal the corresponding charges of the M atoms, and we found, in agreement with the experimental results [9], that Ni can be more easily reduced during a HER experiment, while Mn atoms will keep their 2+ oxidation state.

Author Contributions: L.K.: investigation, formal analysis, writing—original draft, software, visualization. F.T.: writing—review and editing. P.B.: supervision, writing—review and editing. All authors have read and agreed to the published version of the manuscript.

Funding: This research was funded by the TU-D doctoral college (TU Vienna).

Institutional Review Board Statement: Not applicable.

Informed Consent Statement: Not applicable.

Data Availability Statement: The data presented in this study are available in insert article.

Conflicts of Interest: The authors declare no conflict of interest.

References

1. Diebold, U. The surface science of titanium dioxide. *Surf. Sci. Rep.* **2003**, *48*, 53–229.
2. Khan, M.M.; Pradhan, D.; Sohn, Y. *Nanocomposites for Visible Light-Induced Photocatalysis*; Springer: Cham, Switzerland, 2017; Volume 101.
3. Ameta, R.; Ameta, S.C. *Photocatalysis: Principles and Applications*; CRC Press: Boca Raton, FL, USA, 2016.
4. Ibhadon, A.O.; Fitzpatrick, P. Heterogeneous photocatalysis: recent advances and applications. *Catalysts* **2013**, *3*, 189–218.
5. Ni, M.; Leung, M.K.; Leung, D.Y.; Sumathy, K. A review and recent developments in photocatalytic water-splitting using TiO_2 for hydrogen production. *Renew. Sustain. Energy Rev.* **2007**, *11*, 401–425.
6. Jafari, T.; Moharreri, E.; Amin, A.S.; Miao, R.; Song, W.; Suib, S.L. Photocatalytic water splitting—The untamed dream: A review of recent advances. *Molecules* **2016**, *21*, 900.
7. Liu, L.; Zhao, H.; Andino, J.M.; Li, Y. Photocatalytic CO_2 reduction with H_2O on TiO_2 nanocrystals: Comparison of anatase, rutile, and brookite polymorphs and exploration of surface chemistry. *ACS Catal.* **2012**, *2*, 1817–1828.
8. Xu, M.; Gao, Y.; Moreno, E.M.; Kunst, M.; Muhler, M.; Wang, Y.; Idriss, H.; Wöll, C. Photocatalytic activity of bulk TiO_2 anatase and rutile single crystals using infrared absorption spectroscopy. *Phys. Rev. Lett.* **2011**, *106*, 138302.
9. Schubert, J.S.; Popovic, J.; Haselmann, G.M.; Nandan, S.P.; Wang, J.; Giesriegl, A.; Cherevan, A.S.; Eder, D. Immobilization of Co, Mn, Ni and Fe oxide co-catalysts on TiO_2 for photocatalytic water splitting reactions. *J. Mater. Chem. A* **2019**, *7*, 18568–18579.
10. Hohenberg, P.; Kohn, W. Inhomogeneous electron gas. *Phys. Rev.* **1964**, *136*, B864.
11. Kohn, W.; Sham, L.J. Self-consistent equations including exchange and correlation effects. *Phys. Rev.* **1965**, *140*, A1133.
12. Hebenstreit, W.; Ruzycki, N.; Herman, G.S.; Gao, Y.; Diebold, U. Scanning tunneling microscopy investigation of the TiO_2 anatase (101) surface. *Phys. Rev. B* **2000**, *62*, R16334–R16336.
13. Alghannam, A.; Muhich, C.L.; Musgrave, C.B. Adatom surface diffusion of catalytic metals on the anatase TiO_2(101) surface. *Phys. Chem. Chem. Phys.* **2017**, *19*, 4541–4552.
14. Wang, Y.; Su, Y.; Zhu, M.; Kang, L. Ni cluster nucleation and growth on the anatase TiO_2(101) surface: A density functional theory study. *RSC Adv.* **2015**, *5*, 16582–16591.
15. Iyemperumal, S.K.; Fenton, T.G.; Gillingham, S.L.; Carl, A.D.; Grimm, R.L.; Li, G.; Deskins, N.A. The stability and oxidation of supported atomic-size Cu catalysts in reactive environments. *J. Chem. Phys.* **2019**, *151*, 054702.

16. Sharma, P.K.; Cortes, M.A.; Hamilton, J.; Han, Y. Surface modification of TiO_2 with copper clusters for band gap narrowing. *Catal. Today* **2019**, *321*, 9–17.
17. Zhou, X.; Dong, H. A Theoretical perspective on charge separation and transfer in metal oxide photocatalysts for water splitting. *ChemCatChem* **2019**, *11*, 3688–3715.
18. Singh, D.J.; Nordström, L. *Planewaves, Pseudopotentials and the LAPW Method*, 2nd ed.; Springer: Berlin, Germany, 2006.
19. Karsai, F.; Tran, F.; Blaha, P. On the importance of local orbitals using second energy derivatives for d and f electrons. *Comput. Phys. Commun.* **2017**, *220*, 230–238.
20. Blaha, P.; Schwarz, K.; Madsen, G.K.H.; Kvasnicka, D.; Luitz, J.; Laskowski, R.; Tran, F.; Marks, L.D. *WIEN2k: An Augmented Plane Wave plus Local Orbitals Program for Calculating Crystal Properties*; Vienna University of Technology: Vienna, Austria, 2018.
21. Blaha, P.; Schwarz, K.; Tran, F.; Laskowski, R.; Madsen, G.K.H.; Marks, L.D. WIEN2k: An APW+ lo program for calculating the properties of solids. *J. Chem. Phys.* **2020**, *152*, 074101.
22. Perdew, J.P.; Ruzsinszky, A.; Csonka, G.I.; Vydrov, O.A.; Scuseria, G.E.; Constantin, L.A.; Zhou, X.; Burke, K. Restoring the density-gradient expansion for exchange in solids and surfaces. *Phys. Rev. Lett.* **2008**, *100*, 136406.
23. Schossberger, F. Über die Umwandlung des Titandioxyds. *Zeitschrift Kristallographie* **1942**, *104*, 358–374.
24. Anisimov, V.I.; Zaanen, J.; Andersen, O.K. Band theory and Mott insulators: Hubbard U instead of Stoner I. *Phys. Rev. B* **1991**, *44*, 943–954.
25. Bader, R.F.W. *Atoms in Molecules: A Quantum Theory*; Oxford University Press: Oxford, UK, 1990.
26. Bader, R.F.W. Atoms in molecules. *Acc. Chem. Res.* **1985**, *18*, 9–15.